

# Electrochemical erasing using polymer lithography editor for the fabrication of photoactive devices

Nathalie Becerra-Mora,<sup>1</sup> Annie Y. Vargas-Lizarazo,<sup>1</sup> Connor Orrison,<sup>2</sup> Monica Barron<sup>3</sup>, Rajesh P Balaraman,<sup>1</sup> and Punit Kohli<sup>1\*</sup>

<sup>1</sup>Department of Chemistry and Biochemistry, Southern Illinois University, Carbondale, IL 62901

<sup>2</sup>Old Dominion University, Norfolk, VA, 23529

<sup>3</sup>Department of Chemistry and Chemical Biology, Indiana University-Purdue University, Indianapolis, Indianapolis, IN 46202

\*Corresponding author: pkohli@chem.siu.edu

## Abstract

Electrochemical erasing of conductive coatings at microscale for the fabrication of functional devices on flexible and hard surfaces is demonstrated. The nanoporous pyramidal-shaped nano- and micro-scale polyacrylamide hydrogel PLE probes allowed delivery of electrochemical etchants to the surface providing on-demand maskless patterning at microscale. Highly efficient erasing (silver and copper metals erasing efficiency  $\approx 100\%$ ), areal erasing rate  $\approx 80 \mu\text{m}^2/\text{s}$ , and pressure dependent spatial erasing feature dimensions between  $3 \mu\text{m}$  to many tens of microns on metal surfaces allowed fabrication of microelectrodes of various geometries. Overall, PLE-based microscale erasing allowed rapid and accessible fabrication of organic

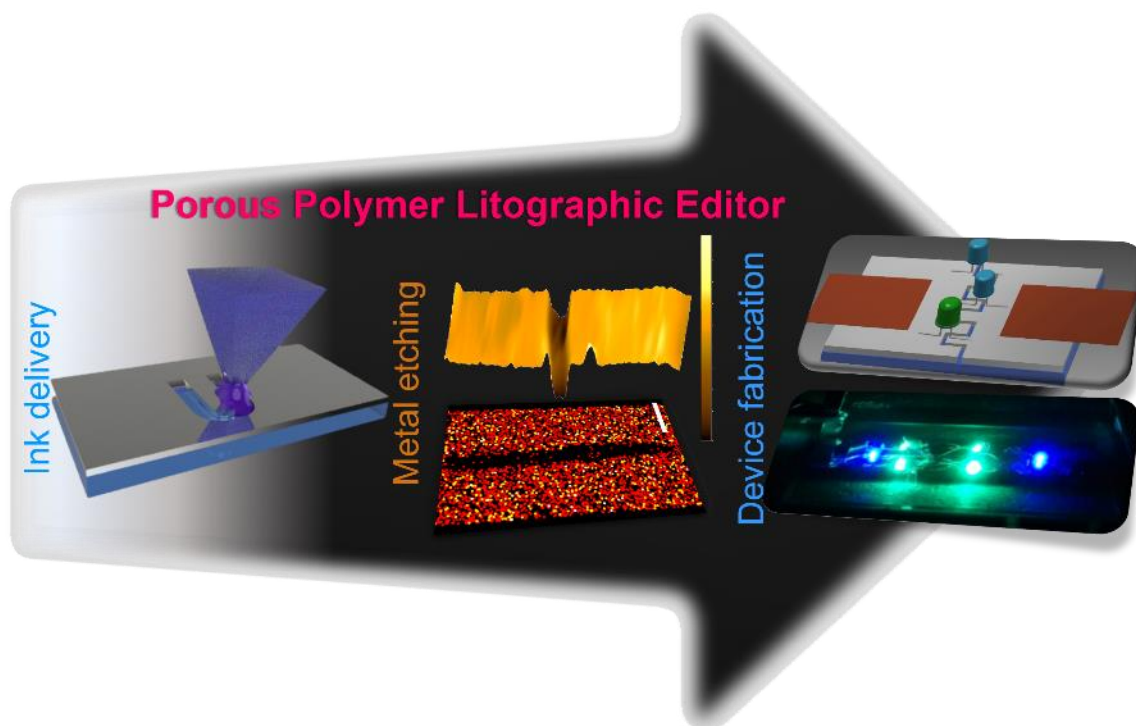
---

This is the author's manuscript of the article published in final edited form as:

Becerra-Mora, N., Vargas-Lizarazo, A. Y., Orrison, C., Barron, M., Balaraman, R. P., & Kohli, P. (2019). Electrochemical Erasing Using a Polymer Lithography Editor for the Fabrication of Photoactive Devices. ACS Applied Electronic Materials.

<https://doi.org/10.1021/acsaelm.9b00099>

1  
2  
3 electron-hole carrier pair based micro-photodetector, as well as the assembly of LED  
4 on flexible and rigid ITO substrates.  
5  
6  
7  
8  
9



32 *Keywords:* Litographic editor, electrochemical etching, hydrogel, device  
33 fabrication, micro-photo-detector  
34  
35

### 36 37 38 **Introduction**

39  
40 Dip-pen nanolithography (DPN)<sup>1-4</sup>, polymer-pen lithography (PPL)<sup>5-7</sup>, micro-contact  
41 printing ( $\mu$ CP)<sup>8</sup>, and nano-fountain pen (NFP)<sup>9-11</sup> have been demonstrated for  
42 selective delivery and patterning of a large number of molecules<sup>2</sup> on a variety of  
43 surfaces<sup>12</sup>. A plethora of studies<sup>3</sup> are published for improving the delivery and the  
44 patterning of a large variety of molecules,<sup>13,14,15-16</sup> the spatial resolution,<sup>7</sup> and  
45 throughput rate<sup>17</sup>. The patterned surfaces and devices fabricated using these  
46 techniques possess a wide range of potential applications in bioengineering<sup>18</sup>,  
47  
48  
49  
50  
51  
52  
53  
54  
55  
56  
57  
58  
59  
60

1  
2  
3 medical diagnostics,<sup>19-20</sup> and electronics industry<sup>21,22</sup>, and the number of studies is  
4  
5 expected to grow further.<sup>23</sup>  
6  
7

8 The tip probe-based deposition using DPN, PPL, and NFP are well-suited for  
9  
10 achieving ultra-high patterning resolution below 100 nm. DPN is capable of  
11  
12 achieving spatial resolution patterning as low as 15 nm over large areas.<sup>24</sup> For large-  
13  
14 scale patterning, a reservoir of molecular ink allows continuous supply of ink. For  
15  
16 example, ink reservoirs containing NFP can allow patterning at large scale without a  
17  
18 need to redeposit ink in the probes.<sup>25</sup> For example, use of a cantilever coated with  
19  
20 PDMS yielded nanostructures within a range of 60-470 nm<sup>26</sup>. The reservoirs have  
21  
22 also allowed storage of a large amount of ink molecules and particles for  
23  
24 deposition.<sup>17</sup> Additionally, control over the patterning area by changing the pen-  
25  
26 substrate contacting area was also demonstrated using soft PDMS probes<sup>27</sup>.  
27  
28 Analogously, hydrogel matrixes can be loaded with a large amount of aqueous-ink  
29  
30 molecules several orders higher concentration as compared to non-porous probes,<sup>28</sup>  
31  
32 allowing the delivery and deposition of molecules over large areas.<sup>29,30</sup>  
33  
34  
35  
36  
37  
38

39 In general, probe-based erasing and patterning requires formation a meniscus  
40  
41 between the probe and the substrate. This is usually achieved when the probe is  
42  
43 brought near a desire surface resulting in the transfer of molecules from the probe  
44  
45 to the surface. In the case of PPL, transfer of ink can occur through the meniscus  
46  
47 at substrate-probe interface, and through direct contact between tip and substrate  
48  
49 as well. This molecule transport mechanism is comparable to the deposition  
50  
51 mechanism involved in  $\mu$ CP. The rate of molecular transport from probe to the  
52  
53 substrate is dependent on the physical and chemical characteristics of the ink<sup>31</sup>,  
54  
55  
56  
57  
58  
59  
60

1  
2  
3 substrate, tip material properties,<sup>32</sup> and environmental conditions such as  
4 temperature and relative humidity.<sup>33</sup> Ink-tip and ink-substrate interactions are key  
5 processes that also affect the size of the patterned features in the probe-based  
6 patterning. Although the concentration difference based-passive diffusion and/or  
7 through fluid dynamics<sup>34</sup> are dominantly used for molecular transport for the surface  
8 patterning, much higher patterning rate (~2-3 orders of magnitude larger than those  
9 observed in the passive transport probe delivery systems) can be accomplished the  
10 application of an external electrical potential stimulus between probe and  
11 substrate.<sup>10, 35</sup>

12  
13  
14 Although the molecular deposition using probe-based techniques is broadly  
15 investigated, the studies describing the selective removal of molecules from surfaces  
16 are limited in the literature. For example, nanoshaving,<sup>36</sup> nanografting,<sup>37</sup> and  
17 electrochemical removal using a conductive atomic force microscope (AFM) tip<sup>38</sup> are  
18 demonstrated for molecular removal and erasing. Because of serial probe  
19 movements at nanometer scale during erasing, these techniques can be expensive  
20 and time-consuming.<sup>39</sup> For example, in the case of nanoshaving and nanodrafting,  
21 the mechanical erasing requires intimate probe-surface contact that may damage  
22 and/or induce defects in probe tips and substrates. Recently, an error rectifying  
23 method using polymer lithography editor (PLE) was introduced, where a soft probe  
24 composed of agarose hydrogel allowed molecular erasing and writing mediated  
25 through a meniscus formed between the probe and substrate.<sup>40</sup> The rectification  
26 process “writing-erasing-rewriting” was demonstrated by “writing” ~10  $\mu\text{m}$   
27 fluorescein array dots on glass substrate. The accuracy of erasing was

1  
2  
3 demonstrated by placing PLE eraser within 700 nm of a given registration spot;  
4  
5 “rewriting” with fluorescein using PLE at the erased area completed the editing  
6  
7 process. The erasing process in PLE involves two major steps: an initial step  
8  
9 involves the solvation of the patterned molecules by solvent molecules transported  
10  
11 from the tip or molecules that are already present on the substrate surface. This is  
12  
13 followed by a second step where solvated molecules diffuse into the nanoporous  
14  
15 PLE tip matrix driven by concentration gradient.<sup>40</sup> Similarly, the writing/rewriting  
16  
17 process was accomplished by transport of the ink molecules through the meniscus  
18  
19 at the PLE probe-substrate interface. PLE was also utilized for the fabrication of the  
20  
21 functional photo-active micro-devices in this study.  
22  
23  
24  
25

26  
27 Manipulation of physical and chemical properties of the conductive and elastomeric  
28  
29 materials has led to the development of flexible electronics devices. These devices  
30  
31 possess a wide range of potential applications including, but not limited to, non-linear  
32  
33 electronic eyeball cameras, deformable LEDs, 3D micro/nano-structures and  
34  
35 functional devices, flexible diagnostic devices for brain surgery, and interfaces for  
36  
37 human-computer control systems and related biointegrated devices.<sup>41-49</sup> The PLE-  
38  
39 based lithography is complementary to many lithographic deposition and patterning  
40  
41 techniques presently used in industry.  
42  
43  
44

45  
46 In this manuscript, we show that polyacrylamide (PAAM) hydrogel PLE probes  
47  
48 delivered electrochemical etchant molecules selectively to carry out reactions at the  
49  
50 microscale level for the functional device fabrication. We demonstrate  
51  
52 electrochemical etching of multi-electrode materials (silver, copper, and indium tin  
53  
54 oxide) for the fabrication of interdigitated electrodes on soft and hard substrates.  
55  
56  
57

1  
2  
3 The interdigitated electrodes were used to fabricate micro-photodetectors using  
4 deposition of organic electron-hole pair (P3HT-bis[60]PCBM) on hard substrates.  
5  
6 Further, the assembling of LED was accomplished using PLE-assisted micro-  
7  
8 electrodes fabricated on both hard and flexible substrates. Using PLE, this work  
9  
10 demonstrates the fabrication of microscale functional devices in wet laboratory  
11  
12 conditions without a need of traditional clean room lithography facilities.  
13  
14  
15

16  
17 Overall, due to selective spatial etching, PLE allows the fabrication of devices on a  
18  
19 variety of substrates including both soft and hard materials and those that may be  
20  
21 susceptible to multi-steps harsh conditions employed in traditional photolithography.  
22  
23 Importantly, PLE provides mask-less on-demand electrochemical etching at the  
24  
25 microscale over large areas in ambient wet conditions. Clean-room conditions are  
26  
27 optional for microscale patterning when utilizing PLE. Thus, the main attractive  
28  
29 feature of the PLE is that through simple programming of a micro-stage with attached  
30  
31 substrate that needs to be patterned allows fabrication of desired patterns at  
32  
33 microscale features under ambient conditions. Thus, the use of PLE based  
34  
35 fabrication can be potentially useful for fast prototyping without the need of extensive  
36  
37 instrumentation and clean room facility.  
38  
39  
40  
41  
42

## 43 **Experimental section**

44  
45  
46 *A.1 Materials.* MCC Primer 80/20 was purchased from Micro Chem. ME 351  
47  
48 (Microdeposit™ 351 Developer) and S1805 photoresist (Microposit™ S1805™  
49  
50 Positive photoresist) were obtained from ROHM and HAAS Electronic Materials,  
51  
52 Massachusetts. Buffered-HF was purchased from Transene Company, Inc.  
53  
54 Danvers, MA. Pyrocatechol (Catechol 99 %) was obtained from Alfa Aesar.  
55  
56  
57

1  
2  
3 Ethylene diamine 99% (extra pure), ammonium persulfate 98% (extra pure),  
4 acrylamide 99%, hydrogen peroxide 30 %, and sulfuric acid were purchased from  
5 Fisher Scientific. Bis-acrylamide was purchased from Amresco, N,N,N',N'-  
6 tetramethylethylenediamine 99% extra pure (TEMED), ferric chloride, and poly(3-  
7 hexylthiophene-2,5-diyl) P3HT (MW 85,000–100,000) were obtained from Sigma  
8 Aldrich. Bis[60]PCBM and potassium permanganate were obtained from TCI and  
9 Mallinckrodt respectively.  
10  
11  
12  
13  
14  
15  
16  
17  
18

19  
20 *A.2. Characterization and methods.* The electronic absorption spectrum of  
21 bis[60]PCBM and P3HT in *o*-dichlorobenzene were acquired using a PerkinElmer  
22 Lambda 25 spectrometer with a slit width of 1 nm. Emission spectroscopy was  
23 performed using a Perkin Elmer LS 55 spectrometer. Both the excitation and  
24 emission slit widths were 3.0 nm, and the scanning speed for the acquisition of the  
25 spectra was 50 nm/min. The photo-induced current (PIC) measurements were  
26 accomplished using Keithley 6487 picoammeter/voltage source. A xenon arc lamp  
27 (300 W) controlled by a power supply (model no. 69907, Newport) provided photo-  
28 excitation for photoelectron-induced studies. The optical characterization of the  
29 hydrogel pen and electrochemical metal erasing were performed using a bright-field  
30 inverted Leica DMIRB microscope.  
31  
32  
33  
34  
35  
36  
37  
38  
39  
40  
41  
42  
43  
44

45  
46 *Scanning Electron Microscopy (SEM) and energy dispersive X-ray spectroscopy*  
47 *(EDS).* SEM was performed using a FEI Quanta FEG 450 SEM equipped with an  
48 EDX MaxX 50 mm<sup>2</sup> Oxford detector controlled using an INCA software. SEM images  
49 and EDS were acquired at an accelerating voltage of 10-20kV. Non-conductive  
50  
51  
52  
53  
54  
55  
56  
57  
58  
59  
60

1  
2  
3 samples for SEM analysis were coated with a silver or gold-palladium layer  
4  
5 (thickness ~100-150 Å).  
6  
7

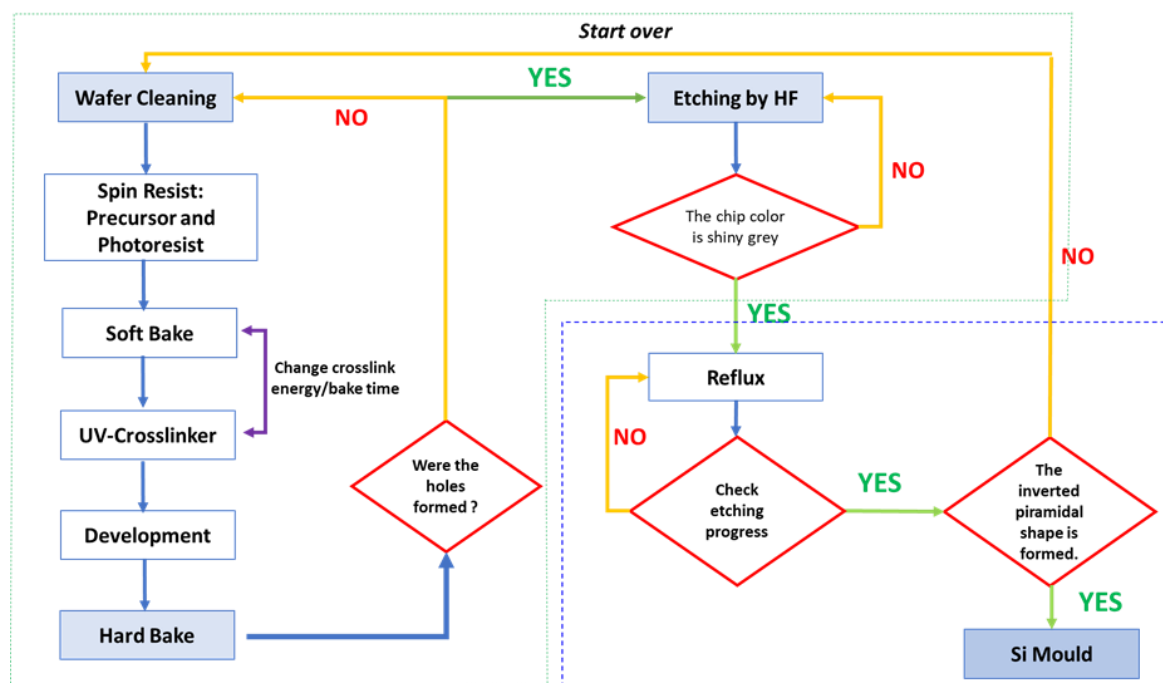
8 *Atomic Force Microscopy.* The AFM measurements were performed using  
9  
10 Autoprobe Thermomicroscopes in contact mode. The microscope was controlled  
11  
12 using ThermoMicroscopes ProScan version 1.6 Beta software. The sample was  
13  
14 probed with a silicon nitride tip MLCT-AUMT-A with a nominal force constant given  
15  
16 by the manufacturer of 30 pN/nm.  
17  
18

## 19 20 *B. Fabrication of PAAM PLE probes.*

21  
22  
23 *B.1 Pyramidal silicon master fabrication using photolithography.* The fabrication of  
24  
25 array pyramidal pores was accomplished using anisotropic etching of Si(100)  
26  
27 plane.<sup>50</sup> To guide future researchers in the fabrication of lithographic patterning, we  
28  
29 provide a detailed flow chart and give some tips that may be helpful for the fabrication  
30  
31 of multiple pyramidal pores (Scheme 1). In addition, with the aim to help readers,  
32  
33 we captured a sequence of images at each key step of the methodology (Fig. S1).  
34  
35 A detailed procedure of the mold fabrication (photolithography and Si anisotropic  
36  
37 etching) can be found in the supporting information.  
38  
39  
40  
41

42 *B2. Fabrication of hydrogel probes.* PAAM hydrogel was chosen because its  
43  
44 mechanical properties and porosity can be modulated by monomer (acrylamide) to  
45  
46 cross-linker (bis-acrylamide) ratio ( $R_{MC}$ ). For example, variation in the  $R_{MC}$  can  
47  
48 provide PAAM with a wide range of Young's modulus, porosity, and pore size<sup>51</sup>.  
49  
50 The porosity of the PAAM hydrogels enables large capacity for hydrophilic material  
51  
52  
53  
54  
55  
56  
57  
58  
59  
60

that can be stored within the pores, and it also facilitates the transfer of solute and solvent from/to pores to/from bulk solution.



**Scheme 1.** Flow chart for the Si master fabrication through photolithography and HF anisotropic etching. Fig. S1 shows the optical micrographs of the wafer and the pores at various stages.

Prior to formation of the PAAM PLE probes, the surface of the Si chips was cleaned using O<sub>2</sub> plasma for 120 s (power 250 W, Ar 80%, 20% O<sub>2</sub>). The hydrogel mixture was prepared as follows: 250 μL of acrylamide (AM, 100 % w/v), 50 μL of bis-acrylamide (bAM, 2 % w/v), and 25 μL of APS (initiator, 10 % w/v) were vigorously mixed in a 2 mL tube. This mixture was kept in an ice bath for 2 minutes and 2 μL of TEMED (catalyst) was added along the inner walls of the tube. A homogeneous distribution of the components in the solution ensured uniform crosslinking and

1  
2  
3 polymerization within the matrix of the hydrogel. 180  $\mu\text{L}$  of this solution was added  
4 promptly to a Si chip template containing sixteen pyramidal shape pores. The PAAM  
5 crosslinking process was rapid and was observed to occur within two minutes of the  
6 mixture into the pores. Once PAAM hydrogel was gelled, it was peeled off from the  
7 template and stored in nanopure water at 4°C until further use. The treatment of the  
8 pore templates was not found to be necessary for the release of the polymer probes  
9 from the templates.  
10  
11  
12  
13  
14  
15  
16  
17  
18  
19

20 *B.3. Micro-scale electrochemical erasing using PLE-based probes.* The micro-  
21 photodetectors on the PLE probe etched interdigitated electrodes were fabricated  
22 by the deposition of an organic electron-hole active pair on the electrodes. Briefly,  
23 sputtered 100 nm thick silver or copper films with a 10 nm thick Cr adhesion layer  
24 on glass slides was used. The metal substrate was placed on a Leica DMRIB  
25 inverted microscope with a Ludl computerized stage that controlled x- and y-direction  
26 movements using an Oasis Blue PCI controller card. The PLE probe was attached  
27 to a z-axis piezoelectric stage, and was brought close to the substrate at a vertical  
28 speed ( $v_z$ ) of 0.1  $\mu\text{m/s}$  with a step size of 150 nm. The erasing process was followed  
29 on an inverted microscope in transmission mode using microscope objectives (10x  
30 and 20x with numerical apertures of 0.25 and 0.40, respectively). The microscope  
31 was equipped with a camera Photometrics CoolSNAP Myo. Briefly, a PAAM PLE  
32 containing either Ag etchant (KI + I<sub>2</sub>, TFS from Transene Inc.) or Cu etchant (Fe(III),  
33 CE-200 Transene Inc.) was allowed to make contact with the metal coating using a  
34 z-axis piezoelectric stage. For ITO etching, an acidic solution of Fe(III) containing  
35 PAAM single pen attached to the z-piezoelectric stage. The PLE probe formed a  
36  
37  
38  
39  
40  
41  
42  
43  
44  
45  
46  
47  
48  
49  
50  
51  
52  
53  
54  
55  
56  
57  
58  
59  
60

1  
2  
3 liquid meniscus between the probe and substrate delivering redox etchants to the  
4  
5 substrate that resulted in the erasing (etching) of the metal coating. The relative  
6  
7 humidity for all the experiments was  $40\pm 10\%$ . For copper- and silver-coated  
8  
9 substrates, the chromium adhesion layer in-between Cu or Ag and glass was  
10  
11 removed by dipping the substrates in an alkaline potassium permanganate solution.  
12  
13 After removal of the chromium etchant, the substrate was rinsed with copious  
14  
15 amounts of water and ethanol, then it was followed by air drying. The complete  
16  
17 removal of metal coating was confirmed by measuring the electrical resistance of the  
18  
19 electrodes. The open circuit was assumed when the electrical resistance of the  
20  
21 fabricated electrode was  $>1\text{ G}\Omega$ .  
22  
23  
24  
25

26  
27 *B.4. Fabrication of micro-photo-detector.* An active layer of a light harvesting  
28  
29 mixture composed of poly(3-hexylthiophene-2,5-diyl) (P3HT) and bis-phenyl C<sub>60</sub>-  
30  
31 butyric acid methyl ester (bis[60]PCBM) was deposited on the microelectrode.  
32  
33 Briefly, 0.02 g of P3HT dissolved in 2 mL of *o*-dichlorobenzene was mixed with 0.016  
34  
35 g of bis[60]PCBM solution in 2 mL of *o*-dichlorobenzene. 3  $\mu\text{L}$  of the active layer  
36  
37 was deposited by spin-coating on the electrodes at 500 rpm for 10 seconds (step 1)  
38  
39 followed by 1000 rpm for 10 s (step 2). The spin-coated surfaces were checked for  
40  
41 uniformity using optical microscopy. The absorption, emission spectroscopy and  
42  
43 atomic force microscopy were used to characterize the active layer of the micro-  
44  
45 photodetector devices.  
46  
47  
48  
49

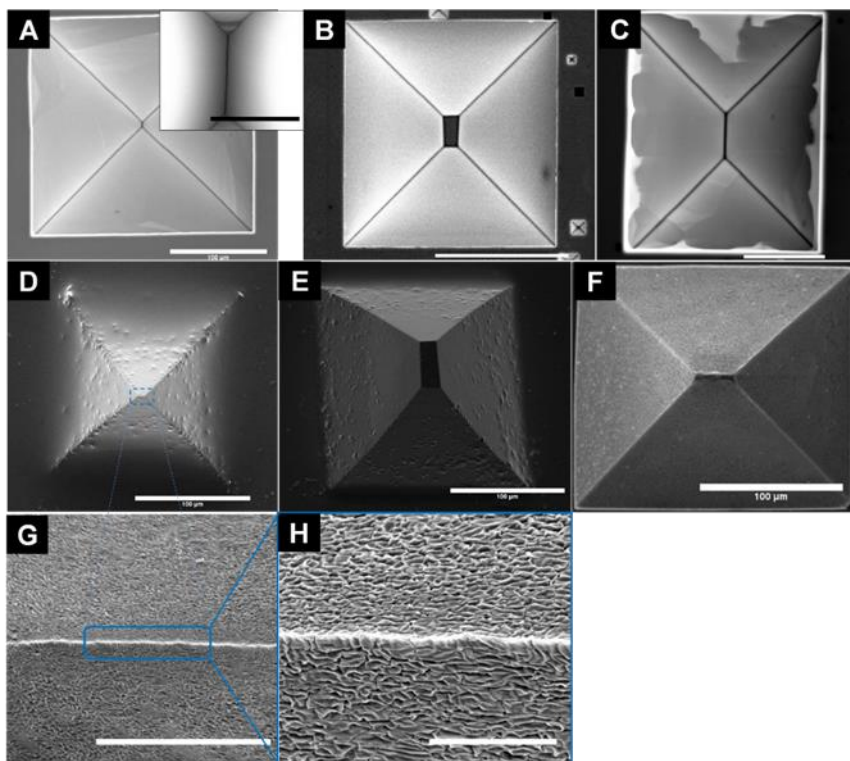
50  
51 *B.5. LED assembly on PLE fabricated flexible electrodes.* The conductive flexible  
52  
53 ITO-PET substrates (Delta Technologies) of dimensions 4 mm x 13 cm were rinsed  
54  
55 with ethanol and air-dried prior to the probe etching for the fabrication of electrodes.  
56  
57  
58  
59  
60

1  
2  
3 The film attached to a glass slide was placed on the x- and y-motorized stage of the  
4 microscope using a double-sided tape (3M). PLE hydrogel probes attached to a  
5 piezoelectric stage were soaked in an acidic solution of Fe(III) for at least one hour  
6 prior to the experiment. The PLE was brought in contact to the conductive substrate.  
7  
8 The stage was programmed to move with x- and y- speed ( $v_x$  and  $v_y$ ) of 5  $\mu\text{m/s}$  in a  
9 zig-zig pattern (175  $\mu\text{m}$  in x-direction followed by 200  $\mu\text{m}$  in the y-direction) that  
10 resulted in inter-digitated electrodes for the fabrication of the micro-  
11 photodetectors/LED assembly. The metal erasing was performed from edge to edge  
12 for an etched length of  $\sim 4$  mm. The electrical resistance across the inter-digitated  
13 electrodes yielded an open circuit system ( $>1\text{G}\Omega$ ), indicating that the conductive  
14 material in the patterned area was completely removed. Blue and green LEDs were  
15 glued to the film using silver paint followed by putting a thin layer of super glue for  
16 mechanical stability. Copper tape was connected to the two electrodes on the  
17 flexible ITO substrates for attaching devices to an external power supply (GW  
18 INSTEK GPS-18500). A forward bias of 3.0 V was used for all LED experiments.  
19 Stretching studies on the flexible electrodes was carried out by mounting the LED-  
20 ITO-PET setup on an x-y stage. The LED glued using silver paint and copper tape  
21 on PLE etched devices were then connected to Keithley 6487 (applied potential  
22 ( $V_{\text{appl}}$ ) = 3 V). Current and resistance measurements were monitored as the device  
23 was stretched with increments of 2 mm.  
24  
25  
26  
27  
28  
29  
30  
31  
32  
33  
34  
35  
36  
37  
38  
39  
40  
41  
42  
43  
44  
45  
46  
47  
48

## 49 **Results and Discussion**

50  
51  
52 *Pyramidal pores in Si wafers.* Fig. 1 shows SEM images of the pyramidal pores  
53 obtained using Si anisotropic etching in an aqueous pyrocatechol-ethylenediamine  
54  
55  
56  
57

1  
2  
3 mixture. The activation energy for alkaline etching of Si(100) planes is smaller than  
4 that of Si(111) planes<sup>52</sup> that results in higher etching rate for the Si(100) planes  
5 compared to the Si(111) planes. The size and shape of the pyramidal pore depends  
6 upon the shape and size of the exposed silicon during etching. The square-shaped  
7 exposed areas on photo-resist coated Si wafers resulted in sharp pointed pores  
8 when the etching is proceeded to completion. However, the square-shaped tip  
9  
10  
11  
12  
13  
14  
15  
16



17  
18  
19  
20  
21  
22  
23  
24  
25  
26  
27  
28  
29  
30  
31  
32  
33  
34  
35  
36  
37  
38  
39  
40  
41  
42  
43 **Figure 1.** SEM of typical pyramidal pores and PAAM PLE probes. (A) SEM of line-  
44 shaped. Inset shows a larger magnification image of the tip, the tip width is roughly  
45 50 nm (scale bar=4 μm). (B) and (C) pyramidal pores in Si wafers were fabricated  
46 using anisotropic etching of Si in basic solution. Corresponding nanoporous PAAM  
47 PLE probes of line-shaped (D) and rectangular-shaped (E) and (F) were formed by  
48 filling the pores up with PAAM solution and peeling them away from the Si wafer.  
49 Higher-resolution SEMs of (D) are shown in (G) and (H) show that the tip is ~300 nm  
50 x 700 nm (scale bars are 10 and 5 μm, respectively). The scale bar is 100 μm for  
51 images (A) to (F).  
52  
53  
54  
55  
56  
57  
58  
59  
60

1  
2  
3 pyramidal pores were resulted when the etching was stopped prior to its completion.  
4  
5 Similarly, the rectangular-shaped exposed areas on photo-resist coated Si wafers  
6  
7 yielded sharp line or rectangular shaped pores depending upon extend of etching.  
8  
9  
10 For example, a line-shaped tip was obtained when the exposed area at the start of  
11  
12 the etching is rectangular. However, stopping the etching process at an intermediate  
13  
14 stage prior to a complete etching resulted in a rectangular tip pyramidal pore. Fig. 1  
15  
16 shows both the line shaped and rectangular shaped pores in the Si wafer produced  
17  
18 in our experiments. The tip ( $d_t$ ) of the PLE probes ranged between 300 nm to 64  $\mu\text{m}$   
19  
20 depending upon the extent of the Si(100) etching. Sub-micron PLE line-shaped  
21  
22 probe of 300 nm wide and 700 nm length was also prepared (Figs. 1D and 1H).  
23  
24 These sharp tips were used for the fabrication of the PAAM hydrogel probes for the  
25  
26 high- resolution erasing applications.  
27  
28  
29

30  
31 A nanoporous hydrogel PLE probes were prepared by radical polymerization of AM  
32  
33 (monomer, M) with bAM (crosslinker, C) in presence of APS (initiator) and catalyst  
34  
35 TEMED. The ratio of C to M ( $R_{MC}$ ) was 0.2% in all PLE probes (Eqs. 1 and 2). In  
36  
37 practice, both the storage capacity and mechanical properties of the probe needs to  
38  
39 be considered for patterning requirements. Therefore, the composition of the PLE  
40  
41 probes should be carefully adjusted depending upon the erasing and writing  
42  
43 requirements.  
44  
45

$$T (w/v) = \frac{M+C}{V} \times 100\% \quad \text{Eq. 1}$$

$$C \left( \frac{w}{w} \right) = \frac{C}{M+C} \times 100\% \quad \text{Eq. 2}$$

46  
47  
48  
49  
50  
51  
52  
53 After crosslinking of the polymer in the pyramidal pores and subsequent peeling off  
54  
55 from the Si wafer yielded an optically clear array of polymer probes. Porous PAAM  
56  
57

1  
2  
3 probes were imaged using SEM after lyophilization of the hydrogel for a closer  
4 visualization at high spatial resolution of the porous matrix (Figs. 1 G-H). Although  
5 SEM provided nanoscale resolution of the pores, the pore size distribution within the  
6 PLE matrix from SEM images cannot accurately obtained. This is because of low  
7 contrast limitation for our samples below 10 nm and a lack of high resolution  
8 information deep inside of the PLE matrix. Further, the harsh vacuum conditions  
9 used during imaging also affected the pore and interpore dimensions. Finally, a thin  
10 conductive metal coating (~10-15 nm) sputtered for SEM imaging may also damage  
11 or distort the sample at nanoscale. Due to these reasons, although the SEM  
12 information on the porous PLE is highly useful, the spatial information below 10 nm  
13 however should be interpreted with caution.  
14  
15  
16  
17  
18  
19  
20  
21  
22  
23  
24  
25  
26  
27  
28

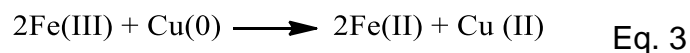
29 *Patterning using PLE electrochemical metal erasing.* Patterning and deposition of  
30 metals to fabricate micro-electronic components at the micro- and nano-scale  
31 frequently utilize wet chemical etching of noble metals including Au, Ag, and Cu<sup>53</sup>.  
32 One reason for their extensive use in electronic and opto-electronic devices is their  
33 low electrical resistivity and relatively high chemical inertness to chemical attacks.  
34 Metal etching usually involves dissolution of metal using a liquid-phase etchant on  
35 selective parts of the metal whereas a masked metal area is protected against the  
36 etching. The photoresist masked metal using photolithography followed by isotropic  
37 metal etching is shown to achieve spatial resolution as high as 50 nm<sup>54</sup>.  
38  
39  
40  
41  
42  
43  
44  
45  
46  
47  
48

49 Device miniaturization in the electronic industry demands development and  
50 enhancement in the state-of-the-art of tools and techniques for microfabrication.  
51 Several techniques including FIB<sup>55</sup> is capable meeting the industry requirements in  
52  
53  
54  
55  
56  
57  
58  
59  
60

1  
2  
3 terms of resolution, yet multiplexing, throughput rate of these techniques are not  
4  
5 implemented at the industrial scale for device fabrication. Further, in general,  
6  
7 appropriate clean room facilities are required for above-mentioned lithography and  
8  
9 photolithographic patterning techniques where sub-micron resolution is required.  
10  
11 However, the equipment and maintenance costs (including, that of clean room)  
12  
13 associated with the above mentioned tools can be extremely high which warrants for  
14  
15 alternatives fabrication tools that would help in lowering the cost of device  
16  
17 fabrication.  
18  
19

20  
21 In this report, PLE-based editing is demonstrated for on-demand etching and  
22  
23 patterning of metal (Cu, Ag, and ITO) and other technologically important materials  
24  
25 with features at microscale. Further, we also demonstrate here the fabrication of  
26  
27 functional micro-photodetectors and LED assembly on soft and hard surfaces that  
28  
29 were patterned at microscale using PLE probes.  
30  
31

32  
33 *Electrochemical copper erasing using PLE probes.* Fe(III) is industrially used for the  
34  
35 etching of the Cu metal. Cu(0)/Fe(III) redox reaction provides water soluble,  
36  
37 predominantly FeCl<sub>2</sub><sup>+</sup> and Cu(II) species.<sup>56</sup> The overall redox reaction usually  
38  
39 represented by Eq. 3 is thermodynamically accessible ( $E_o = 0.43$  V):  
40  
41

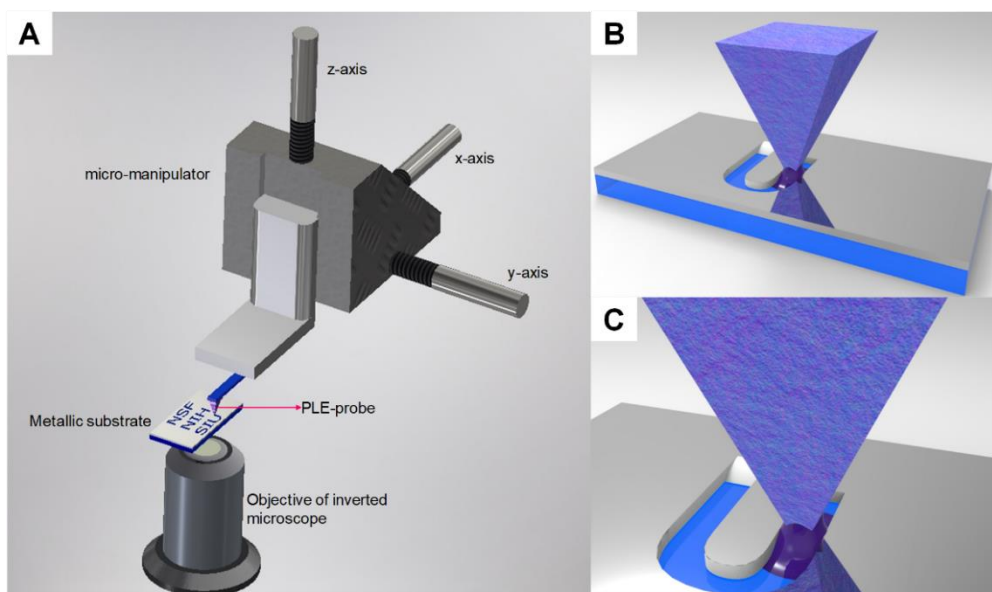


45  
46 Importantly, redox reaction Cu(0)/Fe(III) is kinetically fast and follows first order rate  
47  
48 constant with  $R_{\text{etching}} = 0.2-0.33 \text{ mg Cu} \cdot \text{kg/cm}^2 \cdot \text{s} \cdot \text{mol Fe(III)}$  for  $0 < [\text{Fe(III)}] < 0.8$   
49  
50 mol/kg.<sup>57-58</sup>  
51  
52

53  
54 Scheme 2 shows the set-up used to perform PLE experiments. The PLE probe was  
55  
56 attached to a glass cantilever that was then fixed to a piezoelectric stage (step size  
57  
58

1  
2  
3 of 150 nm). By programming the x-y stage as described in the *Materials and*  
4  
5 *Experimental* section a desired erasing pattern was achieved by delivering etchant  
6 molecules contained in the probe matrix to the substrate while moving the stage  
7  
8  
9  
10  
11  
12  
13 used in the microscale erasing of various metallic surfaces for the devices  
14  
15 fabrication.

16  
17  
18 Fig. 2 presents a line array patterns of ten electrochemical etched lines fabricated  
19  
20 on a 100 nm copper coated glass, using a rectangular PLE probe impregnated with  
21  
22 Fe(III) (probe tip dimension was 500 nm x 110 $\mu$ m). Figs. S3 and S4 show EDS color  
23  
24 mapping and spectra of PLE probes loaded with Ag, Cu, and ITO etchants. For line  
25  
26 mapping and spectra of PLE probes loaded with Ag, Cu, and ITO etchants. For line  
27  
28 patterns formed in Fig. 2, the Fe(III) etchant concentration, etching time ( $\tau_e$ ), relative  
29  
30 humidity (RH), and temperature (T) were 3% (w/w), 30 s, 40 $\pm$ 10%, and 25 $^{\circ}$ C,  
31  
32 respectively. The width and length of the line shaped patterns were 2.7 $\pm$ 0.7  $\mu$ m and  
33  
34 112 $\pm$ 2.5  $\mu$ m (n=9), respectively suggesting the microscale features with a narrow-  
35  
36 etched pattern distribution can be obtained using PLE probes in wet lab settings.  
37  
38



1  
2  
3  
4  
5  
6 **Scheme 2.** (A) Schematic of the set-up used for PLE-based erasing. The PLE  
7 probe is attached to a glass cantilever which is fixed to a piezoelectric micro-  
8 manipulator. (B) The relative movement between the substrate and PLE probe  
9 loaded with a redox-etchant allowed a desired pattern formation (C) A close up  
10 image of the meniscus formed between the PLE probe and the substrate.  
11

12 It is noticeable that the size of the patterned features is larger than the tip dimension.  
13

14 For example, the patterns formed in these studies were about five times wider (~2.7  
15  $\mu\text{m}$ ) than the width of the PLE probe tip of 500 nm (Fig. 2). This is consistent with  
16  
17 our previous studies where the PLE fabricated patterns were also larger than the  
18 size of the probe.<sup>59</sup> The contribution of various factors including meniscus size at  
19 tip-substrate interface, molecular interaction between the tip and surface,  
20 mechanical properties of the probe tip, and ink-transport characteristics ultimately  
21 determine the size of the patterned features.<sup>34</sup> Further, parameters such as relative  
22 humidity, temperature and ink physico-chemical characteristics also contribute to the  
23 formation and size of the water meniscus.<sup>60</sup>  
24  
25  
26  
27  
28  
29  
30  
31  
32  
33  
34  
35

36 In Scheme 2C, the meniscus at the PLE probe-substrate interface is shown for  
37 illustrative purposes. However, at this point, we do not know the exact size of the  
38 meniscus at the PLE tip-substrate interface. However, we estimate the meniscus at  
39 the tip-substrate interface larger than the size of the tip. The erasing process is  
40 through a diffusion-based mechanism where the redox etchant from the PLE probe  
41 transports etchant to the substrate.<sup>59</sup> Thus, the PLE erasing is similar to DPN  
42 lithography where the solvated ink molecules diffused to the patterning surface  
43 through meniscus at the tip-substrate interface. Finally, the erasing pattern size  
44 using PLE etching depends upon many experimental parameters, and probe and ink  
45  
46  
47  
48  
49  
50  
51  
52  
53  
54  
55  
56  
57  
58  
59  
60

characteristics (please see above for more discussion). More detailed studies are needed to fully understand the contributions of each parameter on the erasing pattern dimension.

Cu etching with PLE probes was also confirmed by EDS and AFM analysis. EDS elemental Cu and Si concentration represented by  $[Cu]_{EDS}$  and  $[Si]_{EDS}$  in the EDS mapping confirmed the depletion of Cu (Figs. 2B-2E). The orange and purple shaded EDS maps show elemental Cu and Si respectively (Figs. 2C and 2D), whereas the elemental Cu and Si overlap is shown in Fig. 2E. Under our experimental conditions, the electrochemical Cu(0)/Fe(III) redox reaction was dependent upon both the etching time ( $\tau_{etching}$ ) and Fe(III) concentration. Fig. 2F shows that decrease in the  $[Cu]_{EDS}/[Si]_{EDS}$  ratio with  $\tau_{etching}$  for both  $[Fe(III)]=0.3\%$  and 3% conditions.  $[Cu]_{EDS}/[Si]_{EDS} \approx 0.1$  suggested that copper was not completely etched but it remained constant for  $\tau_{etching} > 45s$  and  $[Fe(III)]=0.3\%$  (Fig. 2). The etching rate of Cu(0) was found to increase with  $[Fe(III)]=3\%$  containing PLE probes – a complete Cu etching was observed for  $\tau_{etching}=60s$  as confirmed using EDS. The quantitative Cu(0) volumetric etching rate ( $R_{vol,etching}$ ) was followed by AFM measurements (Fig. 2G).  $R_{vol,etching} = \frac{\partial A \times d_f}{\partial t}$  was estimated by erased metal area ( $\partial A$ ) from SEM measurements, known thickness ( $d_f=100$  nm) of the coating and erasing time. We estimated  $R_{vol,etching} \approx 0.5 \mu m^3/s$  and  $1.0 \mu m^3/s$  with  $[Fe(III)]=0.3\%$  and 3% respectively for a rectangular-shaped PLE probes of dimension  $500$  nm x  $110 \mu m$ .

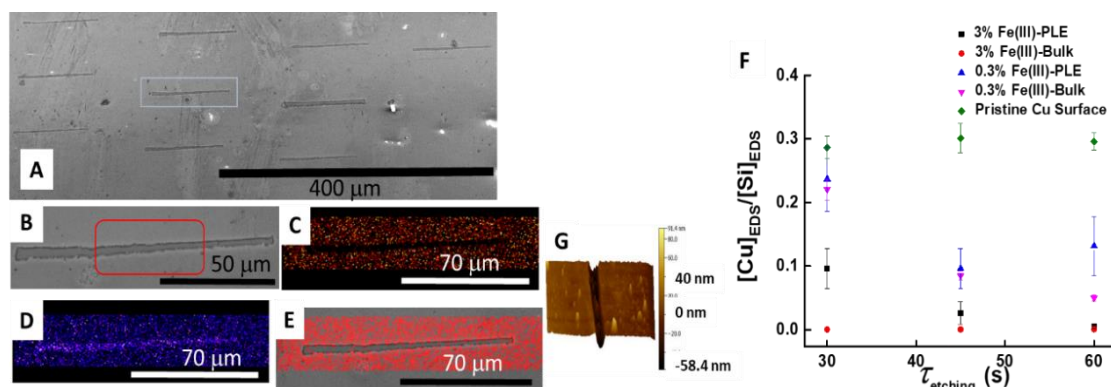
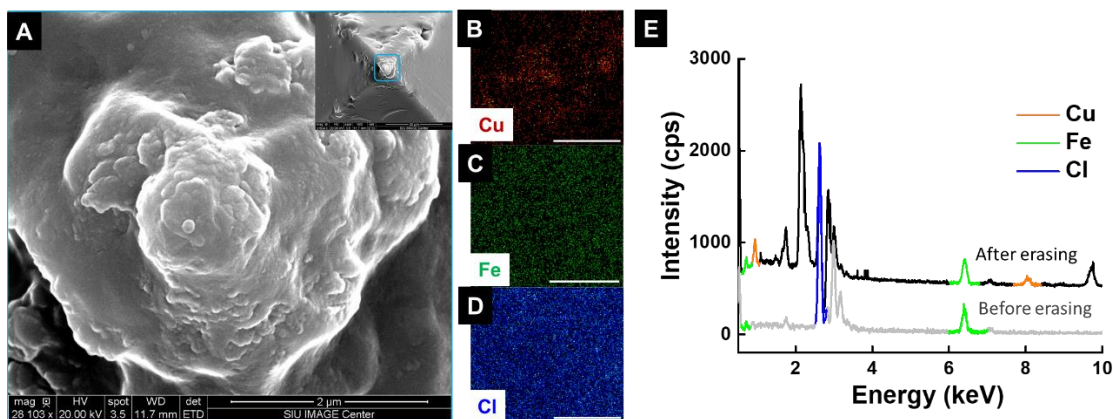


**Figure 2.** Copper erasing and pattern formation. PLE was used to erase copper and formation of patterns on copper surfaces for the fabrication of the micro-photo-detectors. (A) An SEM of an array of rectangular shaped Cu erased patterns using a PLE probe. The electrochemical erasing was performed using a PLE probe with tip dimension of 500 nm x 110 μm;  $\tau_e=30$ s; RH=40±10%; T=25°C; and [Fe(III)]=3%. The length and width of the erased patterns were 112±2.5 μm and 2.7±0.7 μm (n=9) respectively. (B) A higher magnification SEM of an erased pattern in blue rectangle in (A). The EDS mapping analysis shows complete depletion of element Cu (C) with increase in the Si signal (D). (E) An overlap of elemental Cu and Si signals. The comparison of the  $R_{etching,vol}/\tau_{etching}$  for the PLE probe and bulk etching is shown in (F).  $R_{etching,vol}$  for the PLE were 0.4 μm<sup>3</sup>/s and 0.90 μm<sup>3</sup>/s for [Fe(III)]=0.3% and 3% respectively, whereas the bulk etching rate was four times larger for [Fe(III)]=3%. (G) An AFM of an etched pattern of depth of ~45 nm.

We performed additional experiments to study the etching rates of the copper in bulk conditions and compared this with PLE probe etching. We found that the etching rate was more than four times faster in the bulk solution for [Fe(III)]=3% as compared to the PLE etching ([Fe(III)]=3%, Fig. 2F). However, there were insignificant differences in the etching rates between PLE-based and bulk etching for [Fe(III)]=0.3%. These results imply that there are differences between the PLE-probe and bulk etching rate depending upon the etchant conditions and that the PLE locomotion speed needs to be adjusted for optimum etching. Although more thorough studies are needed to investigate why this difference would be. One of the possibilities is that at higher etchant conditions beyond a limiting value for the bulk case, the local etchant concentration and mass transport are sufficiently high that

1  
2  
3 allowed enhanced etching rate in comparison to the PLE-based etching.  
4  
5 Additionally, we also investigated the mechanical stability of the polymer PLE  
6  
7 probes. After utilizing the PLE probes for three erasing cycles with  $>30,000 \mu\text{m}^2$  Cu  
8  
9 erasing, insignificant damage to the probe was evident from the SEM imaging.

10  
11  
12  
13 The coating thickness employed in the micro-electronics, batteries, and other  
14  
15 devices are comparable to those employed here, suggesting that the results in these  
16  
17 studies are relevant to the etching of conductive coatings employed in the micro-  
18  
19 electronics and other related industries. Importantly, we routinely and reproducibly  
20  
21 obtained spatial features of  $<10 \mu\text{m}$  in width and up to many cm in length using PLE  
22  
23 probes. These results are useful for device fabrication because of the microscale  
24  
25 erased feature dimension we can obtain at relatively high throughput rate. With  
26  
27 optimization of the PLE probe and etching conditions (etching time, temperature,  
28  
29 and etchant concentration), finer etching patterns of sub-micron dimensions with  
30  
31 appropriate high throughput rate are feasible.  
32  
33  
34  
35  
36



50  
51 **Figure 3.** (A) A higher magnification SEM image of a PLE tip loaded with  
52 [Fe(III)]=0.3% after Cu etching (magnification~28 k, scale bar=2  $\mu\text{m}$ ). Inset of (A)  
53 shows a lower magnification image. EDS color mapping in the PLE probe with Cu  
54 (B, maroon), etchant molecules Fe (C, green), and Cl (D, blue), scale bars=2  $\mu\text{m}$ .  
55 (E) The EDS spectrum obtained at the tip of the PLE probe before (bottom) and after  
56 (top) Cu etching. Energy peaks at 2.98 keV (Ag  $L\alpha$ ), 2.12 keV (Au  $M$ ), 9.712 keV  
57

1  
2  
3 (Au  $L\alpha$ ), and 2.828 keV (Pd  $L\alpha$ ) came from conductive coating performed on the  
4 PLE probe. The presence of Cu x-ray peaks in the spectrum suggested the diffusion  
5 of the aqueous copper species into the porous PLE probe.  
6  
7  
8

9  
10 An interesting question arises when metal is removed from the substrate during PLE  
11 erasing, what is the fate of the reaction products following the erasing process? In  
12 the PLE process, erasing is performed at the probe-substrate interface through an  
13 electrochemical reaction between an etchant and metal (M(0)). The formation of  
14 solvated  $M^{n+}$  through the redox reaction allows erasing of M(0). The solvated  $M^{n+}$   
15 ions diffuse into the probe and to the surrounding areas. In order to address this  
16 question, EDS and SEM were used to examine the PLE probe before and after  
17 copper etching. A total area of  $\sim 28,716 \mu\text{m}^2$  was etched using  $[\text{Fe(III)}]= 0.3\%$  and  
18  $\text{RH}=40\%$  at  $25 \text{ }^\circ\text{C}$ . Low etchant concentration in the PLE probe and large surface  
19 erasing were found to be suitable for investigating the fate of solvated Cu(II) after  
20 the erasing process. Erasing of small areas ( $<10,000 \mu\text{m}^2$ ) were not successful in  
21 the detection of solvated Cu(II) in the PLE probe, probably due to the EDS detection  
22 limit and low concentration of the Cu(II) into the probe.  
23  
24  
25  
26  
27  
28  
29  
30  
31  
32  
33  
34  
35  
36  
37  
38  
39

40 The EDS spectra gathered at the tip of the PLE probe showed accumulation of Cu  
41 speciation after etching within the PLE matrix (Fig. 3). Fe  $K\alpha$  and  $L\alpha$  with energy of  
42 6.398 keV and 0.705 keV respectively, and that of Cl  $K\alpha$  2.621 keV are shown in Fig.  
43 3E. The energy peaks of 0.93 and 8.04 keV corresponding to Cu  $L\alpha$  and  $K\alpha$  peaks  
44 respectively confirmed the presence of Cu in the PLE probe (Fig. 3E). It is important  
45 to note that the EDS analysis is semi-quantitative in the present studies. Therefore,  
46 we cannot over-emphasize the EDS data presented here, although, qualitatively  
47  
48  
49  
50  
51  
52  
53  
54  
55  
56  
57  
58  
59  
60

1  
2  
3 EDS results provided a clear evidence of erased Cu species in the probe. Further,  
4 at this point, it is not entirely clear if all the solvated Cu species diffused into the  
5 probe. More extensive quantitative studies are underway to clarify these questions  
6 and will be reported in a future manuscript.  
7  
8  
9  
10

11  
12 The diffusion of the reaction products into PLE matrix can have implication on the  
13 erasing process. In the initial stage, the effect of the diffusion of the products into  
14 the PLE matrix is expected to be low because the etchant concentration difference  
15 (which is the driving force) is large for etchant to diffuse out of the probe. Also, the  
16 low product concentration is expected to have an insignificant effect on the erasing  
17 rate. However, large area erasing may significantly increase the reaction product  
18 concentration in polymer matrix, which, in principle, can hinder the etchant diffusion  
19 out of the probe to the meniscus present at the probe-substrate interface. It appears  
20 that careful studies are needed to fully understand the effect of diffusion of the  
21 reaction products on PLE erasing.  
22  
23  
24  
25  
26  
27  
28  
29  
30  
31  
32  
33  
34  
35

36 *Translocation of PLE probes for metal patterning.* Whereas Cu etching in the  
37 previous section was accomplished using PLE probe-copper surface contact, the  
38 relative motion between the PLE and the substrate was demonstrated for patterning  
39 on Ag and ITO surfaces. Fig. S5 shows the microscale Ag erasing patterns  
40 accomplished by moving [I<sub>2</sub>-KI]=18% (w/v) containing PLE probes at a speed of 5  
41 μm/s. A rectangular-shaped PLE probe (dimension = 11 μm x 24 μm) was used for  
42 these experiments. The SEM and EDS measurements of the erased patterns  
43 indicated that the complete removal of Ag from the surface was achieved after two  
44 probe passes (cycles) over the pattern. One PLE erasing cycle did not appear to  
45  
46  
47  
48  
49  
50  
51  
52  
53  
54  
55  
56  
57  
58  
59  
60

1  
2  
3 etch Ag completely but ~97% silver remained on the surface after one erasing cycle.  
4  
5 The EDS mapping of elemental Ag and Si confirmed complete erasing after three or  
6  
7 more erasing PLE cycles (Fig. S6). Patterns with width and length  $\sim 32.2 \pm 11.6 \mu\text{m}$   
8  
9 and  $\sim 1330 \mu\text{m}$  (1.33 mm) respectively, an erased area of  $\sim 0.043 \text{ mm}^2$  was  
10  
11 accomplished which yielded areal speed ( $R_{\text{area,etching}}$ ) and  $R_{\text{vol,etching}}$  of  $\approx 80 \mu\text{m}^2/\text{s}$  and  
12  
13  $8 \mu\text{m}^3/\text{s}$  respectively.  $R_{\text{area,etching}} = w \times v_{\text{probe}}$  and  $R_{\text{vol,etching}} = w \times v_{\text{probe}} \times d$ ; here,  $w$ ,  $d$ ,  
14  
15 and  $v_{\text{probe}}$  were width of the pattern, thickness of silver coating, and speed of the  
16  
17 probe, respectively. Assuming complete Ag erasing was accomplished in two  
18  
19 erasing cycles (Fig. S6) at  $v_{\text{probe}} = 5 \mu\text{m}/\text{s}$ , the observed Ag  $R_{\text{vol,etching}}$  was ~8 times  
20  
21 that of  $R_{\text{vol,etching}}$  for the Cu where the PLE probe-surface contact mechanism was  
22  
23 employed. The  $R_{\text{vol,etching}}$  depends upon the probe size, concentration and  
24  
25 temperature of the redox etchant, and etchant-metal redox kinetics rate. For  
26  
27 example, larger probe size delivers larger volume of the etchants that will result in  
28  
29 enhanced  $R_{\text{vol,etching}}$ . Similarly, as shown for the Cu etching, the etchant  
30  
31 concentration is also an important parameter that affects the etching rate. In our  
32  
33 experiments, the area of the PLE probe used for the Ag erasing was ~5 times larger  
34  
35 than the area of the probe used for the Cu etching which may account for enhanced  
36  
37 etching rate. Further, the etchant-metal redox kinetics consideration is also  
38  
39 important for fully utilization of the probe-based pattern formation. Under optimized  
40  
41 conditions, a larger etching rate than those demonstrated here can be obtained by  
42  
43 controlling the etchant concentration and temperature, probe dimension, and mass-  
44  
45 transport and kinetics of the metal-etchant reaction.  
46  
47  
48  
49  
50  
51  
52  
53  
54  
55  
56  
57  
58  
59  
60

1  
2  
3 *Fabrication of functional micro-photodetector and LED devices using PLE patterned*  
4 *electrodes.* The interdigitated electrodes were fabricated by translocating 18% w/v  
5 aqueous [KI-I<sub>2</sub>]-complex containing PLE probes over Ag-coated glass wafers at a  
6 speed of 5 μm/s. Fig. 4A shows a schematic of the interdigitated electrode based  
7 micro-photodetector fabricated using the PLE erasing. The zig-zag probe movement  
8 of the PLE over metallic coating resulted in interdigitated electrodes with conductive  
9 metal electrode width and spacing of 50 μm and 150 μm respectively (inset Fig. 4B).  
10 After Ag etching, the electrical resistance of the electrode increased from <10 Ω to  
11 >1 GΩ (reliable limiting electrical resistance of our multimeter was 1 GΩ) suggesting  
12 that the Ag erasing was successful. These results were also confirmed by the EDS  
13 measurements (Fig. S6). An electron donor-acceptor pair of P3HT and bis[60]PCBM  
14 of 1% and 0.8% concentrations respectively were spin-coated on the interdigitated  
15 electrodes. The films composed of only P3HT and bis[60]PCBM, and that of P3HT-  
16 bis[60]PCBM mixture were also characterized using AFM (Figs. S7 and 4C). The  
17 emission spectra of P3HT before and after addition of acceptor in the solution phase  
18 indicated an emission quenching efficiency of ~45% (Fig. S8). These results are  
19 consistent with previous studies suggesting strong donor-acceptor interactions, and  
20 charge transfer between excited state P3HT and bis[60]PCBM.<sup>61</sup> Figure 4B shows  
21 the experimental set-up used for the acquisition of photo-induced current (PIC). Fig.  
22 4D shows typical PIC-time responses of a typical micro-photodetector device with  
23 light "ON" and "OFF". A solar simulator (AM 1.5) under ambient wet laboratory  
24 conditions was used for all photo-induced studies. With photon irradiation, the PIC  
25 increases sharply exhibiting both the rise ( $\tau_{rise}$ ) and decay times ( $\tau_{decay}$ ) <500 ms.

The device response was found to be stable for less than five “ON-OFF” cycles; the PIC signal response decreased significantly after >10 cycles. This decrease in the PIC signal is attributed to photo-degradation of the active organic layer.

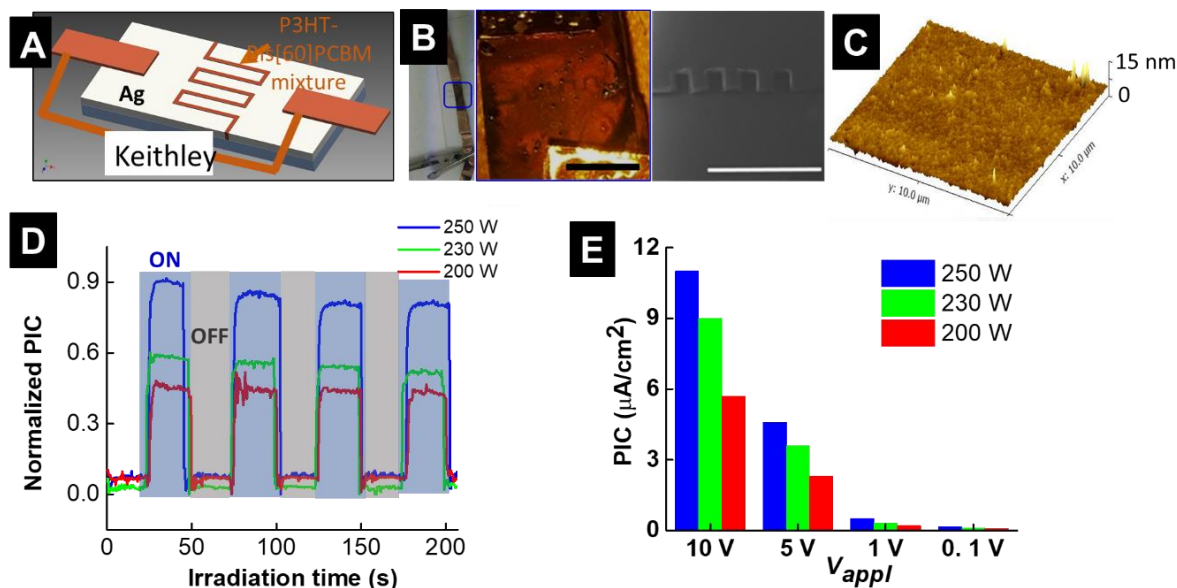


**Figure 4.** Micro-photodetector fabricated using PLE-based patterning of silver interdigitated electrodes. (A) A schematic of a micro-photodetector prepared by erasing silver in a zig-zag pattern thereby fabricating an interdigitated electrode and spin coating an electron donor-acceptor pair on the electrode (brown zig-zag line). Two copper electrodes were attached to the pattern substrate and connected to electric potential using Keithley 6487. (B) The optical photograph (left) and higher magnification optical photograph (middle) of a micro-photodetector assembly in the blue square. The zig-zag patterns on the electrodes are visible in (B). The dark-reddish color comes from the deposition of the donor-acceptor mixture. An SEM image of the patterned electrode (right, scale bar 2 mm). (C) An AFM of P3HT-bis[60]PCBM mixture deposited on the photodetector. (D) A typical PIC-time response of the micro-photodetector for three different powers (200 W, 230 W, and 250 W). The measured photon intensity at 534 nm (Newport Model: 818-SL) for 200 W, 230 W, and 250 W were 142 mW/cm<sup>2</sup>, 220 mW/cm<sup>2</sup>, and 240 mW/cm<sup>2</sup> respectively. (E) Normalized PIC- $V_{appl}$  dependence for the micro-photodetector at three different photon intensities.

Fabrication and testing of devices were performed in wet lab conditions in air (21% oxygen and humidity between ~50%). Oxygen is singlet in its ground state, and is an excellent quencher for molecules in the excited state.<sup>62</sup> Both P3HT and PCBM

1  
2  
3 are known to oxidize and degrade under photo-irradiation conditions. Specifically,  
4 the photo-degradation of P3HT is a light-initiated radical mechanism where the  
5 concentration of the quenched sites increases with the photo-oxidation.<sup>63</sup> Similarly,  
6 PCBM can undergo a series of oxidation when photo-radiated which acts as electron  
7 traps as shown by experimental and DFT studies.<sup>64</sup> The degradation of the  
8 performance of the devices such as ours can be minimized by hermetically sealing  
9 the devices with materials that eliminate (or significantly reduce) the transport of  
10 oxygen, water, and other performance degrading species.

11  
12 Interestingly, the PIC signal depends on the photo-excitation power ( $P$ ) and the  
13 applied voltage ( $V_{appl}$ ) across two electrodes. PIC-photo-excitation power and PIC-  
14  $V_{appl}$  dependences are shown in Figs. 4D and 4E respectively. In general, higher  
15 photon intensity consistently resulted in larger PIC. For example, PIC was ~ 2 times  
16 when  $P=250$  W than when  $P=200$  W. The PIC enhancement at higher lamp power  
17 is attributed to increase in photo-charge generation leading to enhanced PIC. More  
18 dramatic PIC- $V_{appl}$  dependence was observed under same photon intensity  
19 conditions (Fig. 4D). For example,  $PIC_{10,1} = \frac{PIC_{10}}{PIC_1}$  was  $>20$  for all the photon  
20 intensities (200 W, 230 W, and 250 W) tested under our experimental conditions.  
21  $PIC_{10,1}$  is a measure of influence of applied potential, and it is defined as ratio PIC at  
22  $V_{appl}=10$  V to PIC at  $V_{appl}=1$  V. Similarly,  $PIC_{5,1}$  and  $PIC_{1,0.1}$  were  $>9$  and  $>2.5$   
23 respectively for our experimental conditions. In fact,  $PIC_{10,0.1} > 65$  for all the photon  
24 power tested in our experiments. The strong PIC- $V_{appl}$  dependence is not surprising  
25 for randomly dispersed donors and acceptors in the inhomogeneous film where  
26 significant losses due to charge recombination and charge trapping, and other  
27  
28  
29  
30  
31  
32  
33  
34  
35  
36  
37  
38  
39  
40  
41  
42  
43  
44  
45  
46  
47  
48  
49  
50  
51  
52  
53  
54  
55  
56  
57  
58  
59  
60

1  
2  
3 charge loss mechanisms exist.<sup>65</sup> The application of an external electric field  
4  
5 drastically decreased the charge recombination and other losses in the device by  
6  
7 forcing the electrons and holes to transport to opposite appropriate electrodes,  
8  
9 thereby, dramatic enhancing the PIC signal at higher  $V_{appl}$ .

12 *LED device assembly on flexible electrodes.* ITO coated flexible polyester (PET)  
13  
14 substrates (1 cm x 2.7 cm) were also patterned using PLE probes soaked in acidic  
15  
16 0.2 M Fe(III). Etching of ITO with acidic Fe(III) is thermodynamically favorable with  
17  
18 a reported activation energy of  $56 \pm 5$  kJ/mol.<sup>66</sup> The Fe(III) containing PLE probes  
19  
20 were translocated at a speed of 5  $\mu\text{m/s}$  over the ITO surface. Under these  
21  
22 experimental conditions, multiple PLE probe erasing cycles were needed to  
23  
24 completely etch ITO from the surface. The electrical resistance-number of erasing  
25  
26 cycles dependence is shown in Fig. 5A. The electric resistance (R) of the ITO  
27  
28 surface increased from 500  $\Omega$  to >50 M $\Omega$  after four erasing passes for an etched line  
29  
30 of  $\sim 200$   $\mu\text{m}$  x 1 cm line suggesting successful ITO erasing (Fig. 5A). A schematic  
31  
32 and a typical working device with six LEDs (four green and two blue) mounted on  
33  
34 the PLE etched ITO substrate are shown in Figs. 5B and 5C, respectively. We  
35  
36 examined the working behavior of an LED assembled on a flexible ITO-PET  
37  
38 substrate by mounting it on a mechanical station for stretching experiments (Figs.  
39  
40 5D, 5E, and S9). Stretching and relaxation of the unstrained state in the first cycle  
41  
42 did not result in a significant change in electrical resistance ( $R_{ext}$ ) under strain ( $\varepsilon$ ) up  
43  
44 to  $\varepsilon$  up to 4.5% (two-way black arrows) (Fig. 5F). A second stretching cycle with  
45  
46  $\varepsilon=4.5\%$  (two-way red arrows) led to increase in  $R_{ext}$  by an order of magnitude which  
47  
48 however returned to the original value after relaxed to  $\varepsilon=3\%$  showing limited  
49  
50  
51  
52  
53  
54  
55  
56  
57  
58  
59  
60

electrical reversibility of the PLE fabricated devices on ITO coated polyester substrates. For  $\varepsilon=7.6\%$ , however,  $R_{ext}>1\text{ G}\Omega$  was observed. This is due to tearing of the ITO-PET substrates that resulted in the destruction of the conductive pathways for charge transport through the devices.

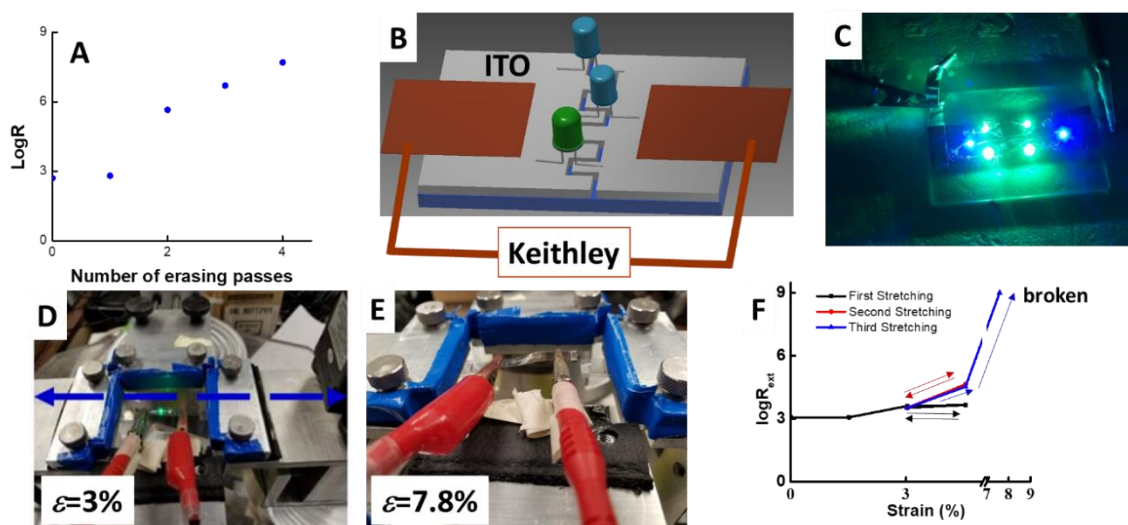


**Figure 5.** Testing of the LED assembly on the PLE fabricated ITO electrodes. (A) LogR-number of erasing passes dependence for the ITO electrodes. Here, R represents the electric resistance of the ITO electrode as a function of number of PLE erasing cycles. (B) Schematic of an LED assembly on ITO electrodes. (C) Four green and two blue LED assembled on an electrode fabricated across an ITO electrode that was fabricated using locomotion of a PLE probe impregnated with acidic Fe(III). The optical photographs of the LED devices assembled on flexible electrodes that were stretched with  $\varepsilon=3\%$  (D) and  $7.8\%$  (E). (F)  $\log R_{ext}-\varepsilon$  dependence indicated that the electrical resistance was not affected significantly for  $\varepsilon=3.3$  but the  $R_{ext}$  increase exponentially at  $\varepsilon>4.5\%$ . The device was damaged at  $\varepsilon=7.5\%$ .

The performance of the devices fabricated in this study was limited by the short-range extension failure due to material selection. With appropriate selection of base materials such as PDMS or PDMS-urethane composites, Rogers and Bao's groups recently demonstrated working devices that can be stretched larger strain  $\varepsilon$  values up to or  $>250\%$ .<sup>43, 45, 67</sup> More extensive studies are currently underway for the

1  
2  
3 fabrication of highly stretchable functional devices based on PLE for wearable  
4 pressure and motion sensing applications.  
5  
6

7  
8 It is instructive to discuss the PLE in light of other lithography techniques widely used  
9 in the industry and academia. The surface selective patterning can be accomplished  
10 using many currently available tools including coated-AFM tips, focused ion beam  
11 (FIB), and electron beam lithography (EBL). For example, the selective removal of  
12 materials from a surface using AFM tips are demonstrated in the literature<sup>68</sup>.  
13  
14 Importantly, AFM can remove materials from a surface through a mechanical  
15 process. However, this causes damage to the probe because of the physical contact  
16 between the tip and the surface, and the probe may need to be replaced if it is blunt  
17 due to damage. Similarly, FIB and electron lithography allows removal of materials  
18 and patterning at a high-resolution (<100 nm). However, the equipment and  
19 operating cost of these two instruments is high; many institutes and resource-limited  
20 countries cannot afford these expensive instruments. The PLE probe utilizes  
21 polymer and contains a liquid interface meniscus that reduces the friction during the  
22 locomotion of the probe. However, as demonstrated in this and in a previous  
23 manuscript,<sup>59</sup> an electrochemical reaction facilitates the erasing process which can  
24 be many orders larger than the mechanical erasing of hard materials. Because  
25 chemical reaction performed at the microscale, a large number of materials are  
26 accessible for erasing at microscale. Further, multiple materials can be erased  
27 simultaneously, or a given material within a matrix of a composite made up of many  
28 species can also be erased. This opens new possibilities for fabricating new  
29 materials with spatial control at microscale level. Finally, the usage of a hydrogel  
30  
31  
32  
33  
34  
35  
36  
37  
38  
39  
40  
41  
42  
43  
44  
45  
46  
47  
48  
49  
50  
51  
52  
53  
54  
55  
56  
57  
58  
59  
60

1  
2  
3 ensures that the amount of ink enclosed within the polymeric matrix is several orders  
4  
5 of magnitude higher than the dry weight of the polymer.  
6  
7

8 It is also important to consider the resolution and throughput rate of erasing using  
9  
10 AFM, FIB, EBL, and that of PLE probes. The resolution of writing and erasing using  
11  
12 AFM, FIB, and electron beam is 2-3 orders better than the patterns made using the  
13  
14 PLE probes. This is a direct consequence of the difference between the AFM and  
15  
16 PLE probe size.<sup>59</sup> Similarly, the electron and ion beams in FIB and EBL respectively  
17  
18 allow much higher resolution erasing than that demonstrated in this study. Further  
19  
20 studies may allow decrease in the erasing features using PLE (probably through  
21  
22 sharper tip and through control of the experimental conditions). Additionally, the  
23  
24 meniscus characteristics and experimental parameters such as humidity also  
25  
26 influence the feature size of the patterns. Throughput rate (erasing and deposition  
27  
28 rate) of the PLE based patterning is many orders of magnitude larger than those  
29  
30 patterns composed using AFM, FIB, and EBL tools. This is because of the large  
31  
32 differences in the probe/beam size. Finally, the erasing process demonstrated in  
33  
34 this report is accomplished using an electrochemical reaction at much larger area  
35  
36 which are practically impossible to accomplish using AFM-based probes with the  
37  
38 same erasing speed. Overall, PLE, AFM, FIB, and EBL provide complementary  
39  
40 tools that have potential applications in a wide field including microelectronics,  
41  
42 biosensors, medical, and life-science.  
43  
44  
45  
46  
47  
48  
49

## 50 **Conclusions**

51  
52  
53 We demonstrated the fabrication of functional devices based on interdigitated  
54  
55 electrodes synthesized using probe-based etching of metallic coatings. Three  
56  
57

1  
2  
3 different metallic coatings (Ag, Cu, and ITO) on both hard and soft surfaces were  
4  
5 erased and patterned using diffusion-based etchant delivery to the metal coating in  
6  
7 contact mode between substrate and PLE. The translocation of PLE over a metallic  
8  
9 coating allowed microscale erasing (etching) of metallic coating on demand in one-  
10  
11 step process. Based on etchant concentration, PLE probe speed, and metal  
12  
13 thickness, the microscale erasing features with minimum pattern size of 2.7  $\mu\text{m}$  was  
14  
15 accomplished with etching rates of  $\sim 8 \mu\text{m}^3/\text{s}$ . Functional micro-photodetector and  
16  
17 LED assemblies were fabricated on flexible and hard conductive interdigitated  
18  
19 electrodes composed using PLE probes. Overall, the PLE allowed on-demand fast  
20  
21 patterning of films of multiple metals with microscale features on both the soft and  
22  
23 hard substrates for the fabrication of functional devices.  
24  
25  
26  
27  
28

### 29 **Acknowledgements**

30  
31 We would like to thank Prof. Kyle Plunkett for providing us a sample of P3HT, and  
32  
33 Prof. P. Sivakumar for the use of his photometer. We also thank anonymous  
34  
35 reviewers for their constructive comments that made the manuscript stronger.  
36  
37

### 38 **Associated content**

39  
40 Scanning electron and optical micrographs of Si chip during photolithographic  
41  
42 process. Detailed description of photolithography and Si anisotropic etching. SEM  
43  
44 and EDS mapping/spectrum of PAAM pen editor loaded with etchants. SEM and  
45  
46 EDS mapping of erased patterned silver using commercial etchant. Silver removal  
47  
48 efficiency in atomic % obtained using EDS. AFM characterization of PCBM and  
49  
50 P3HT films. Absorption and emission spectrum of P3HT and composite  
51  
52 P3HT:PCBM. Photograph of the mechanical stage used for mechanical tests.  
53  
54  
55  
56  
57

## Author Information

### Corresponding Author

\*E-mail: pkohli@chem.siu.edu

### Author Contributions

The manuscript was written through contributions of all authors. All authors have given approval to the final version of the manuscript.

### Funding Sources

National Science Foundation: CHE 0748676, CHE 0959568, and DMR 1757954; and National Institutes of Health (GM 106364). CO and MB were supported through an NSF-REU award (DMR 1757954).

### Notes

The authors declare no competing financial interests.

### References

1. Salaita, K.; Wang, Y.; Mirkin, C. A., Applications of dip-pen nanolithography. *Nature Nanotechnology* **2007**, *2*, 145.
2. Piner, R. D.; Zhu, J.; Xu, F.; Hong, S.; Mirkin, C. A., "Dip-Pen" nanolithography. *Science (New York, N.Y.)* **1999**, *283* (5402), 661-3.
3. Ginger, D. S.; Zhang, H.; Mirkin, C. A., The evolution of dip-pen nanolithography. *Angewandte Chemie (International ed. in English)* **2004**, *43* (1), 30-45.
4. Braunschweig, A. B.; Huo, F.; Mirkin, C. A., Molecular printing. *Nature chemistry* **2009**, *1* (5), 353-8.
5. Eichelsdoerfer, D. J.; Liao, X.; Cabezas, M. D.; Morris, W.; Radha, B.; Brown, K. A.; Giam, L. R.; Braunschweig, A. B.; Mirkin, C. A., Large-area molecular patterning with polymer pen lithography. *Nature protocols* **2013**, *8* (12), 2548-60.
6. Huo, F.; Zheng, Z.; Zheng, G.; Giam, L. R.; Zhang, H.; Mirkin, C. A., Polymer pen lithography. *Science (New York, N.Y.)* **2008**, *321* (5896), 1658-60.
7. Hedrick, J. L.; Brown, K. A.; Kluender, E. J.; Cabezas, M. D.; Chen, P. C.; Mirkin, C. A., Hard Transparent Arrays for Polymer Pen Lithography. *ACS Nano* **2016**, *10* (3), 3144-8.
8. Xia, Y.; Whitesides, G. M., SOFT LITHOGRAPHY. *Annual Review of Materials Science* **1998**, *28* (1), 153-184.
9. Kim, K.-H.; Moldovan, N.; Espinosa, H. D., A Nanofountain Probe with Sub-100 nm Molecular Writing Resolution. *Small (Weinheim an der Bergstrasse, Germany)* **2005**, *1* (6), 632-635.

10. Loh, O. Y.; Ho, A. M.; Rim, J. E.; Kohli, P.; Patankar, N. A.; Espinosa, H. D., Electric field-induced direct delivery of proteins by a nanofountain probe. *Proceedings of the National Academy of Sciences* **2008**, *105* (43), 16438.
11. Moldovan, N.; Keun-Ho, K.; Espinosa, H. D., Design and fabrication of a novel microfluidic nanoprobe. *Journal of Microelectromechanical Systems* **2006**, *15* (1), 204-213.
12. Rogers, J. A.; Nuzzo, R. G., Recent progress in soft lithography. *Materials Today* **2005**, *8* (2), 50-56.
13. Menard, E.; Meitl, M. A.; Sun, Y.; Park, J.-U.; Shir, D. J.-L.; Nam, Y.-S.; Jeon, S.; Rogers, J. A., Micro- and Nanopatterning Techniques for Organic Electronic and Optoelectronic Systems. *Chemical Reviews* **2007**, *107* (4), 1117-1160.
14. Lenhert, S.; Sun, P.; Wang, Y.; Fuchs, H.; Mirkin, C. A., Massively Parallel Dip-Pen Nanolithography of Heterogeneous Supported Phospholipid Multilayer Patterns. *Small (Weinheim an der Bergstrasse, Germany)* **2007**, *3* (1), 71-75.
15. Wang, W. M.; Stoltenberg, R. M.; Liu, S.; Bao, Z., Direct Patterning of Gold Nanoparticles Using Dip-Pen Nanolithography. *ACS Nano* **2008**, *2* (10), 2135-2142.
16. Corletto, A.; Yu, L.; Shearer, C. J.; Gibson, C. T.; Shapter, J. G., Direct-Patterning SWCNTs Using Dip Pen Nanolithography for SWCNT/Silicon Solar Cells. *Small (Weinheim an der Bergstrasse, Germany)* **2018**, *14* (16), e1800247.
17. Huang, L.; Braunschweig, A. B.; Shim, W.; Qin, L.; Lim, J. K.; Hurst, S. J.; Huo, F.; Xue, C.; Jang, J. W.; Mirkin, C. A., Matrix-assisted dip-pen nanolithography and polymer pen lithography. *Small (Weinheim an der Bergstrasse, Germany)* **2010**, *6* (10), 1077-81.
18. Kumar, R.; Weigel, S.; Meyer, R.; Niemeyer, C. M.; Fuchs, H.; Hirtz, M., Multi-color polymer pen lithography for oligonucleotide arrays. *Chemical Communications* **2016**, *52* (83), 12310-12313.
19. Kumar, R.; Bonicelli, A.; Sekula-Neuner, S.; Cato, A. C.; Hirtz, M.; Fuchs, H., Click-Chemistry Based Allergen Arrays Generated by Polymer Pen Lithography for Mast Cell Activation Studies. *Small (Weinheim an der Bergstrasse, Germany)* **2016**, *12* (38), 5330-5338.
20. Xie, Z.; Chen, C.; Zhou, X.; Gao, T.; Liu, D.; Miao, Q.; Zheng, Z., Massively Parallel Patterning of Complex 2D and 3D Functional Polymer Brushes by Polymer Pen Lithography. *ACS Applied Materials & Interfaces* **2014**, *6* (15), 11955-11964.
21. Chung, S.-W.; Ginger, D. S.; Morales, M. W.; Zhang, Z.; Chandrasekhar, V.; Ratner, M. A.; Mirkin, C. A., Top-Down Meets Bottom-Up: Dip-Pen Nanolithography and DNA-Directed Assembly of Nanoscale Electrical Circuits. *Small (Weinheim an der Bergstrasse, Germany)* **2005**, *1* (1), 64-69.
22. Lee, T.-W.; Jeon, S.; Maria, J.; Zaumseil, J.; Hsu, J. W. P.; Rogers, J. A., Soft-Contact Optical Lithography Using Transparent Elastomeric Stamps and Application to Nanopatterned Organic Light-Emitting Devices. *Advanced Functional Materials* **2005**, *15* (9), 1435-1439.
23. O'Connell, C. D.; Higgins, M. J.; Moulton, S. E.; Wallace, G. G., Nano-bioelectronics via dip-pen nanolithography. *Journal of Materials Chemistry C* **2015**, *3* (25), 6431-6444.
24. Mirkin, C. A.; Hong, S.; Demers, L., Dip-pen nanolithography: controlling surface architecture on the sub-100 nanometer length scale. *Chemphyschem* **2001**, *2* (1), 37-39.
25. Hwang, K.; Shin, C.; Mingwu, R.; Lee, S.-H.; Kim, H.-m., Design of a nano-printer based on AFPN (Active Fountain Pen Nano-lithography) using switch control. *Journal of Mechanical Science and Technology* **2011**, *25* (4), 977-985.
26. Zhang, H.; Elghanian, R.; Amro, N. A.; Disawal, S.; Eby, R., Dip Pen Nanolithography Stamp Tip. *Nano Letters* **2004**, *4* (9), 1649-1655.
27. Liao, X.; Braunschweig, A. B.; Mirkin, C. A., "Force-feedback" leveling of massively parallel arrays in polymer pen lithography. *Nano letters* **2010**, *10* (4), 1335-1340.
28. Jaeger, R. D.; Gleria, M., *Inorganic polymers*. Nova Science Publishers: New York, 2007.

- 1  
2  
3 29. Eichelsdoerfer, D. J.; Brown, K. A.; Wang, M. X.; Mirkin, C. A., Role of Absorbed Solvent in  
4 Polymer Pen Lithography. *The Journal of Physical Chemistry B* **2013**, *117* (50), 16363-16368.
- 5 30. Senesi, A. J.; Rozkiewicz, D. I.; Reinhoudt, D. N.; Mirkin, C. A., Agarose-Assisted Dip-Pen  
6 Nanolithography of Oligonucleotides and Proteins. *ACS Nano* **2009**, *3* (8), 2394-2402.
- 7 31. Liu, G.; Zhou, Y.; Banga, R. S.; Boya, R.; Brown, K. A.; Chipre, A. J.; Nguyen, S. T.; Mirkin, C.  
8 A., The role of viscosity on polymer ink transport in dip-pen nanolithography. *Chemical Science*  
9 **2013**, *4* (5), 2093-2099.
- 10 32. and, Y. X.; Whitesides, G. M., SOFT LITHOGRAPHY. *Annual Review of Materials Science*  
11 **1998**, *28* (1), 153-184.
- 12 33. Schwartz, P. V., Molecular Transport from an Atomic Force Microscope Tip: A  
13 Comparative Study of Dip-Pen Nanolithography. *Langmuir* **2002**, *18* (10), 4041-4046.
- 14 34. Urtizbera, A.; Hirtz, M.; Fuchs, H., Ink transport modelling in Dip-Pen Nanolithography  
15 and Polymer Pen Lithography. In *Nanofabrication*, 2016; Vol. 2.
- 16 35. Wang, X.; Wang, X.; Fernandez, R.; Ocola, L.; Yan, M.; La Rosa, A., Electric-Field-Assisted  
17 Dip-Pen Nanolithography on Poly(4-vinylpyridine) (P4VP) Thin Films. *ACS Applied Materials &*  
18 *Interfaces* **2010**, *2* (10), 2904-2909.
- 19 36. Amro, N. A.; Xu, S.; Liu, G.-Y., Patterning Surfaces Using Tip-Directed Displacement and  
20 Self-Assembly. *Langmuir* **2000**, *16* (7), 3006-3009.
- 21 37. Liu, M.; Amro, N. A.; Liu, G.-Y., Nanografting for Surface Physical Chemistry. *Annual Review*  
22 *of Physical Chemistry* **2008**, *59* (1), 367-386.
- 23 38. Li, Y.; Maynor, B. W.; Liu, J., Electrochemical AFM "Dip-Pen" Nanolithography. *Journal of*  
24 *the American Chemical Society* **2001**, *123* (9), 2105-2106.
- 25 39. Tinazli, A.; Piehler, J.; Beuttler, M.; Guckenberger, R.; Tampé, R., Native protein  
26 nanolithography that can write, read and erase. *Nature Nanotechnology* **2007**, *2* (4), 220-225.
- 27 40. Rajasekaran, P. R.; Zhou, C.; Dasari, M.; Voss, K.-O.; Trautmann, C.; Kohli, P., Polymeric  
28 lithography editor: Editing lithographic errors with nanoporous polymeric probes. *Science*  
29 *Advances* **2017**, *3* (6).
- 30 41. Dahl-Young Khang, H. J., Young Huang, John A. Rogers, A Stretchable Form of Single-  
31 Crystal Silicon for High-Performance Electronics on Rubber Substrates. *Science (New York, N.Y.)*  
32 **2006**, *311*, 5.
- 33 42. Kim, D.-H.; Ahn, J.-H.; Choi, W. M.; Kim, H.-S.; Kim, T.-H.; Song, J.; Huang, Y. Y.; Liu, Z.; Lu,  
34 C.; Rogers, J. A., Stretchable and Foldable Silicon Integrated Circuits. *Science (New York, N.Y.)* **2008**,  
35 *320* (5875), 507-511.
- 36 43. Kim, D.-H.; Ghaffari, R.; Lu, N.; Rogers, J. A., Flexible and Stretchable Electronics for  
37 Biointegrated Devices. *Annual Review of Biomedical Engineering* **2012**, *14* (1), 113-128.
- 38 44. Kunnavakkam, M. V.; Houlihan, F. M.; Schlax, M.; Liddle, J. A.; Kolodner, P.; Nalamasu, O.;  
39 Rogers, J. A., Low-cost, low-loss microlens arrays fabricated by soft-lithography replication  
40 process. *Applied Physics Letters* **2003**, *82* (8), 1152-1154.
- 41 45. Rogers, J. A.; Someya, T.; Huang, Y., Materials and Mechanics for Stretchable Electronics.  
42 *Science (New York, N.Y.)* **2010**, *327* (5973), 1603-1607.
- 43 46. Xu, S.; Yan, Z.; Jang, K.-I.; Huang, W.; Fu, H.; Kim, J.; Wei, Z.; Flavin, M.; McCracken, J.;  
44 Wang, R.; Badea, A.; Liu, Y.; Xiao, D.; Zhou, G.; Lee, J.; Chung, H. U.; Cheng, H.; Ren, W.; Banks, A.;  
45 Li, X.; Paik, U.; Nuzzo, R. G.; Huang, Y.; Zhang, Y.; Rogers, J. A., Assembly of micro/nanomaterials  
46 into complex, three-dimensional architectures by compressive buckling. *Science (New York, N.Y.)*  
47 **2015**, *347* (6218), 154-159.
- 48 47. Yugang Sun, W. M. C., Hanqing Jiang, Yonggang Y. Huang and John A. Rogers, Controlled  
49 buckling of semiconductor nanoribbons for stretchable electronics. *Nature Nanotechnology* **2006**,  
50 *1*, 7.
- 51  
52  
53  
54  
55  
56  
57  
58  
59  
60

- 1  
2  
3 48. Hammock, M. L.; Chortos, A.; Tee, B. C. K.; Tok, J. B. H.; Bao, Z., 25th Anniversary Article:  
4 The Evolution of Electronic Skin (E-Skin): A Brief History, Design Considerations, and Recent  
5 Progress. *Advanced Materials* **2013**, *25* (42), 5997-6038.
- 6 49. Sokolov, A. N.; Tee, B. C. K.; Bettinger, C. J.; Tok, J. B. H.; Bao, Z., Chemical and Engineering  
7 Approaches To Enable Organic Field-Effect Transistors for Electronic Skin Applications. *Accounts of*  
8 *Chemical Research* **2012**, *45* (3), 361-371.
- 9 50. Finne, R. M.; Klein, D. L., A Water-Amine-Complexing Agent System for Etching Silicon.  
10 *Journal of The Electrochemical Society* **1967**, *114* (9), 965-970.
- 11 51. Tse, J. R.; Engler, A. J., Preparation of hydrogel substrates with tunable mechanical  
12 properties. *Current protocols in cell biology* **2010**, Chapter 10, Unit 10.16.
- 13 52. Pal, P.; Sato, K., A comprehensive review on convex and concave corners in silicon bulk  
14 micromachining based on anisotropic wet chemical etching. *Micro and Nano Systems Letters* **2015**,  
15 *3* (1), 6.
- 16 53. Choi, T.-S.; Hess, D. W., Chemical Etching and Patterning of Copper, Silver, and Gold Films  
17 at Low Temperatures. *ECS Journal of Solid State Science and Technology* **2015**, *4* (1), N3084-N3093.
- 18 54. Love, J. C.; Paul, K. E.; Whitesides, G. M., Fabrication of Nanometer-Scale Features by  
19 Controlled Isotropic Wet Chemical Etching. *Advanced Materials* **2001**, *13* (8), 604-607.
- 20 55. Cui, A.; Liu, Z.; Dong, H.; Wang, Y.; Zhen, Y.; Li, W.; Li, J.; Gu, C.; Hu, W., Single Grain  
21 Boundary Break Junction for Suspended Nanogap Electrodes with Gapwidth Down to 1–2 nm by  
22 Focused Ion Beam Milling. *Advanced Materials* **2015**, *27* (19), 3002-3006.
- 23 56. Saubestre, E. B., Copper Etching in Ferric Chloride. *Industrial & Engineering Chemistry*  
24 **1959**, *51* (3), 288-290.
- 25 57. Bryce, C.; Berk, D., Kinetics of the dissolution of copper in iron(III) chloride solutions.  
26 *Industrial & Engineering Chemistry Research* **1995**, *34* (4), 1412-1418.
- 27 58. Burrows, W. H.; Lewis, C. T.; Saëre, D. E.; Brooks, R. E., Kinetics of the Copper-Ferric  
28 Chloride Reaction and the Effects of Certain Inhibitors. *Industrial & Engineering Chemistry Process*  
29 *Design and Development* **1964**, *3* (2), 149-159.
- 30 59. Rajasekaran, P. R.; Zhou, C.; Dasari, M.; Voss, K.-O.; Trautmann, C.; Kohli, P., Polymeric  
31 lithography editor: Editing lithographic errors with nanoporous polymeric probes. *Science*  
32 *Advances* **2017**, *3* (6), e1602071.
- 33 60. Rozhok, S.; Piner, R.; Mirkin, C. A., Dip-Pen Nanolithography: What Controls Ink  
34 Transport? *The Journal of Physical Chemistry B* **2003**, *107* (3), 751-757.
- 35 61. Chirvase, D.; Chiguvare, Z.; Knipper, M.; Parisi, J.; Dyakonov, V.; Hummelen, J. C.,  
36 Temperature dependent characteristics of poly(3 hexylthiophene)-fullerene based heterojunction  
37 organic solar cells. *Journal of Applied Physics* **2003**, *93* (6), 3376-3383.
- 38 62. Kautsky, H., Quenching of luminescence by oxygen. *Transactions of the Faraday Society*  
39 **1939**, *35* (0), 216-219.
- 40 63. Hintz, H.; Egelhaaf, H. J.; Lüer, L.; Hauch, J.; Peisert, H.; Chassé, T., Photodegradation of  
41 P3HT–A Systematic Study of Environmental Factors. *Chemistry of Materials* **2011**, *23* (2), 145-154.
- 42 64. Reese, M. O.; Nardes, A. M.; Rupert, B. L.; Larsen, R. E.; Olson, D. C.; Lloyd, M. T.; Shaheen,  
43 S. E.; Ginley, D. S.; Rumbles, G.; Kopidakis, N., Photoinduced Degradation of Polymer and Polymer–  
44 Fullerene Active Layers: Experiment and Theory. *Advanced Functional Materials* **2010**, *20* (20),  
45 3476-3483.
- 46 65. Dasari, M.; Rajasekaran, P. R.; Iyer, R.; Kohli, P., Calligraphic solar cells: acknowledging  
47 paper and pencil. *Journal of Materials Research* **2016**, *31* (17), 2578-2589.
- 48 66. van den Meerakker, J. E. A. M.; Baarslag, P. C.; Scholten, M., On the Mechanism of ITO  
49 Etching in Halogen Acids: The Influence of Oxidizing Agents. *Journal of The Electrochemical Society*  
50 **1995**, *142* (7), 2321-2325.
- 51  
52  
53  
54  
55  
56  
57  
58  
59  
60

- 1  
2  
3 67. Son, D.; Kang, J.; Vardoulis, O.; Kim, Y.; Matsuhisa, N.; Oh, J. Y.; To, J. W. F.; Mun, J.;  
4 Katsumata, T.; Liu, Y.; McGuire, A. F.; Krasen, M.; Molina-Lopez, F.; Ham, J.; Kraft, U.; Lee, Y.; Yun,  
5 Y.; Tok, J. B. H.; Bao, Z., An integrated self-healable electronic skin system fabricated via dynamic  
6 reconstruction of a nanostructured conducting network. *Nature Nanotechnology* **2018**, *13* (11),  
7 1057-1065.  
8  
9 68. Jang, J.-W.; MasPOCH, D.; Fujigaya, T.; Mirkin, C. A., A “Molecular Eraser” for Dip-Pen  
10 Nanolithography. *Small* **2007**, *3* (4), 600-605.  
11  
12  
13  
14  
15  
16  
17  
18  
19  
20  
21  
22  
23  
24  
25  
26  
27  
28  
29  
30  
31  
32  
33  
34  
35  
36  
37  
38  
39  
40  
41  
42  
43  
44  
45  
46  
47  
48  
49  
50  
51  
52  
53  
54  
55  
56  
57  
58  
59  
60